UCLA
UCLA Previously Published Works

Title

Nanocellulose Length Determines the Differential Cytotoxic Effects and Inflammatory Responses in Macrophages and Hepatocytes

Permalink

https://escholarship.org/uc/item/7hf1b808

Journal

Small, 17(38)

ISSN

1613-6810

Authors

Li, Jiulong
Wang, Xiang
Chang, Chong Hyun
et al.

Publication Date

2021-09-01

DOI

10.1002/smll.202102545

Peer reviewed

eScholarship.org Powered by the California Digital Library
University of California

HHS Public Access
Author manuscript
Small. Author manuscript; available in PMC 2022 September 01.

Published in final edited form as:
Small. 2021 September ; 17(38): e2102545. doi:10.1002/smll.202102545.

Nanocellulose Length Determines the Differential Cytotoxic Effects and Inflammatory Responses in Macrophages and Hepatocytes

Jiulong Li,
Center of Environmental Implications of Nanotechnology (UC CEIN), California NanoSystems Institute, University of California, Los Angeles, CA 90095, USA

Xiang Wang,
Center of Environmental Implications of Nanotechnology (UC CEIN), California NanoSystems Institute, University of California, Los Angeles, CA 90095, USA

Division of NanoMedicine, Department of Medicine, University of California, Los Angeles, CA 90095, USA

Chong Hyun Chang,
Center of Environmental Implications of Nanotechnology (UC CEIN), California NanoSystems Institute, University of California, Los Angeles, CA 90095, USA

Jinhong Jiang,
Center of Environmental Implications of Nanotechnology (UC CEIN), California NanoSystems Institute, University of California, Los Angeles, CA 90095, USA

Qi Liu,
Center of Environmental Implications of Nanotechnology (UC CEIN), California NanoSystems Institute, University of California, Los Angeles, CA 90095, USA

Xiangsheng Liu,
Center of Environmental Implications of Nanotechnology (UC CEIN), California NanoSystems Institute, University of California, Los Angeles, CA 90095, USA

Yu-Pei Liao,
Division of NanoMedicine, Department of Medicine, University of California, Los Angeles, CA 90095, USA

Tiancong Ma,
Center of Environmental Implications of Nanotechnology (UC CEIN), California NanoSystems Institute, University of California, Los Angeles, CA 90095, USA

Huan Meng,

---

txia@ucla.edu .

Conflict of Interest
The authors declare no conflict of interest.

Supporting Information
Supporting Information is available from the Wiley Online Library or the author.

Center of Environmental Implications of Nanotechnology (UC CEIN), California NanoSystems Institute, University of California, Los Angeles, CA 90095, USA

Division of NanoMedicine, Department of Medicine, University of California, Los Angeles, CA 90095, USA

Tian Xia
Center of Environmental Implications of Nanotechnology (UC CEIN), California NanoSystems Institute, University of California, Los Angeles, CA 90095, USA

Center of Environmental Implications of Nanotechnology (UC CEIN), California NanoSystems Institute, University of California, Los Angeles, CA 90095, USA

Abstract

Nanocellulose including cellulose nanocrystal (CNC) and cellulose nanofiber (CNF) has attracted much attention due to its exceptional mechanical, chemical, and rheological properties. Although considered biocompatible, recent reports have demonstrated nanocellulose could be hazardous, including serving as drug carriers that accumulate in the liver. However, the nanocellulose effects on liver cells, including Kupffer cells (KCs) and hepatocytes are unclear. Here, we compared the toxicity of nanocellulose with different lengths, including the shorter CNCs (CNC-1, CNC-2, and CNC-3) and longer CNF (CNF-1 and CNF-2), to liver cells. While all CNCs triggered significant cytotoxicity in KCs and only CNC-2 induced toxicity to hepatocytes, CNFs failed to induce significant cytotoxicity due to their minimal cellular uptake. The phagocytosis of CNCs by KCs induced mitochondria ROS generation, caspase-3/7 activation, and apoptotic cell death as well as lysosomal damage, cathepsin B release, NLRP3 inflammasome and caspase-1 activation, and IL-1β production. The cellular uptake of CNC-2 by hepatocytes was through clathrin-mediated endocytosis, and it induced the caspase-3/7-mediated apoptosis. CNC-2 showed the highest levels of uptake and cytotoxicity among CNCs. These results demonstrated the length-dependent mechanisms of toxicity on liver cells in a cell type-dependent fashion, providing information to safely use nanocellulose for biomedical applications.

Keywords

nanocellulose; aspect ratio; liver cells; apoptosis; NLRP3 inflammasome activation

1. Introduction

Cellulose, a linear chain of hundreds to thousands of β(1–4) linked glucose units, is a key structural component (polysaccharide) of the cell walls of plants, algae, and bacteria.[1–3] Nanocellulose, a form of nanostructured cellulose, exists as either cellulose nanocrystal (CNC, also called nanocrystalline cellulose or cellulose nanowhisker), cellulose nanofiber (CNF, also referred to as nanofibrillated cellulose), or bacterial nanocellulose (BC, also referred to as nano-structured cellulose produced by bacteria).[1–6] In light of its various and outstanding advantages including high mechanical strength, stiffness, low weight, high specific surface area, recyclability, bioavailability, biocompatibility, surface tunable chemistry, and rheological properties, nanocellulose has been increasingly considered for applications in papermaking, coatings, food, nanocomposite formulations and reinforcement, as well as in the innovative biomedical fields, including used as drug delivery carriers, 3D culture, antimicrobial materials, and tissue repair and regeneration areas.[2,4–11] The nanocellulose production has a high economic impact and the global nanocellulose market will be projected to grow to approximately $730 million by 2023.[11] This stresses the importance of understanding the toxicity of nanocellulose to generate knowledge that will contribute to predict the health effects from exposure, reduce the risk to humans, or design safer nanocellulose materials for biomedical applications.

Although nanocellulose is generally regarded as safe based on its biocompatibility as well as biodegradability and the great majority of studies have pointed to the absence of significant cytotoxic effects by a vast diversity of CNC samples from different origins and with diverse properties in many mammalian cell lines, recent studies have been reported that nanocellulose displayed the adverse effects *in vitro* and *in vivo*.[11–14] For example, the CNCs in the 200–300 nm length scales have been shown to induce significant lysosomal damage, NLRP3 inflammasome activation as well as IL-1β production in the human myeloid cell line, THP-1.[15] Also, Yanamala *et al.* demonstrated that the generation of oxidative stress, cytotoxicity, and pro-inflammatory by oropharyngeal aspiration of CNCs in mice.[16] The nanocellulose is beneficial for the design of advanced drug delivery systems.[4,9] The liver is the primary target for nanocarriers after intravenous injection or secondary target after environmental exposure to nanomaterials, serving as a major sequestration site for nanoparticles that gain access to the systemic circulation.[17–19] The accumulation of nanocellulose used as drug carriers in the liver will increase the potential of toxicity. For example, the nanocellulose modified with oxalate ester has been reported to induce hepatotoxicity in the liver of rats.[20] However, the detailed mechanism of hepatoxicity induced by nanocellulose at the molecular level is still unclear due to the diverse cell types in the liver. In addition, the differentiation between the adverse impacts of nanocellulose on specific liver cell types has not been reported.

For a better understanding of the nanocellulose effects on the liver, it is necessary to study the interactions of nanocellulose with the major cell types that may encounter nanocellulose after delivery to liver sinusoids from hepatic and portal blood circulations, including Kupffer cells (KCs) and hepatocytes. The Kupffer cell, a major component of the mononuclear phagocyte system (MPS) with a constitution 80−90% of all the tissue macrophages in the body and account for ~15% of all liver cells, plays a major role in phagocytosis of particulate materials, modulation of innate immune responses as well as endotoxin removal.[21–24] Further, KCs also serve as the first line of defense for nanomaterials by phagocytic removal in the liver, which may lead to liver toxicity.[21,22,25,26] Although nanocellulose materials, especially CNCs, have been shown to induce the cytotoxic effects or inflammatory response upon the internalization by macrophages, including THP-1 and RAW 264.7 cells,[11,15] no studies have been performed on nanocellulose effects on KCs. Using various metal oxide, rare earth oxides (REO), and graphene oxide (GO) nanoparticles, we have confirmed that the immortalized Kupffer cell line, KUP5, is a valid cell line for nanotoxicity studies because the results were replicated in primary KCs.[27,28] Hepatocytes, the major functional cells of the liver with a constitution of more than 90% of the total liver volume and as high as 60–80% of the total number of liver cells, perform central roles in protein synthesis, metabolic, endocrine, secretory, detoxification, and excretion of chemical substances in the bile.[29,30] Also, hepatocytes have been shown to take up nanomaterials through clathrin-mediated endocytosis.[25,31] Although studies on nanocellulose toxicity to hepatocytes have been conducted, the results have been conflicting. For example, nanocrystalline celluloses have been shown to induce the loss of cell viability in rainbow trout hepatocytes by Tibor *et al.*,[32] while Madhushree *et al.* found nanofibrillar cellulose hydrogels showed biocompatibility to the human hepatic cell lines including HepaRG and HepG2 cell even at a high concentration and longtime exposure.[33] These seemingly conflicting results likely arise from the differences in the nanocellulose physicochemical properties that affect structure-toxicity relationships. For example, the crystallinity or aspect ratio of nanocellulose has been reported to determine the pro-inflammatory and immune adjuvant effects *in vitro* and *in vivo* with the higher crystallinity index and surface reactivity of nanocellulose showing the stronger effects.[15]

To assess the effects of nanocellulose on the liver cells, we established a nanomaterial library that included the shorter nanocellulose samples, CNCs (including CNC-1, CNC-2, and CNC-3), and longer nanocellulose samples, CNFs (including CNF-1 and CNF-2), provided by the Nanomaterials Health Implications Research (NHIR) Consortium at the National Institute of Environmental Health Sciences (NIEHS) with different lengths in size. This allowed us to systematically evaluate the possible adverse effects of these materials on the KC (KUP5) and hepatocyte (Hepa 1–6) cell lines. Herein, we demonstrated the length- and cell type-dependent apoptotic cell death in the major liver cell types, KUP5 and Hepa 1–6 cells, and then determined the mechanisms that were responsible for the differential cytotoxic responses including ROS generation, caspase-3/7 activation, lysosomal damage and cathepsin B release, NLRP3 inflammasome and caspase-1 activation, and IL-1β release. Furthermore, we evaluated the correlations between nanocellulose physicochemical properties and cellular responses. Additionally, we replicated the results on the length-dependent nanocellulose cytotoxic and pro-inflammatory effects in KUP5 cells in other macrophage cell lines (RAW 264.7 and J774A.1), suggesting that the nanocellulose length-dependent toxic effect was a universal feature to macrophages.

2. Results

2.1 Physicochemical Characterization and Abiotic Assessment of Nanocellulose

The assessment of potential adverse effects of nanocellulose (including shorter nanocellulose samples, CNCs, and longer nanocellulose samples, CNFs) was performed on materials provided by the NHIR Consortium at the NIEHS. The physicochemical characterizations of CNCs and CNFs are detailed in Figure 1 and Tables 1–2. As shown by transmission electron microscopy (TEM) images in Figure 1A, CNCs and CNFs demonstrated different length scales determined by Image J (NIH) software, they were correspondingly named CNC-1, CNC-2, CNC-3, CNF-1, and CNF-2 based on their length from the smallest to the largest in the range of ~150 to ~6700 nm. The nanocellulose samples also showed similar diameters between 20 and 40 nm, except for CNF-1 that was wider than other nanocellulose samples (Table 1). This provides the possibility to compare a structure-activity relationship in the following study. Additionally, their aspect ratios listed in Table 1 were calculated according to the ratio of the length to diameter, demonstrating a similar trend to nanocellulose length.

The hydrodynamic size and zeta potential of the nanocellulose samples in deionized (DI) water as well as in tissue culture medium (Dulbecco's modified Eagle medium, DMEM) were carried out by dynamic light scattering.[15] As listed in Table 2, the hydrodynamic size exhibited a wide range from 110.1 ± 11.2 to 5590.5 ± 3676.4 nm together with a significant difference in the hydrodynamic size of each, furtherly indicating the various lengths among the nanocellulose samples. The nanocellulose samples also displayed negative zeta potential values with a range from −27.93 to −38.73 mV. These values also diminished to approximately −10 mV in the presence of cell culture media, which is likely due to the double-layer formation and protein adsorption on the nanocellulose surfaces.

To characterize the chemical properties of the nanocellulose, we firstly assessed the intrinsic oxidative potential of nanocellulose samples, which reflects the intrinsic capability of nanomaterials to induce ROS generation, using an abiotic H_2DCFDA fluorescence assay kit.[34] For comparison purposes, we also included ZnO particles as a positive control.[35] The results demonstrated a significant increase in DCF fluorescence intensity by CNCs compared to the control, with the highest response being ascribed to the CNC-3, while CNF-1 or CNF-1 did not induce any abiotic ROS generation based on the lower fluorescence intensity than the control (Figure 1B). To assess the effect on abiotic redox equilibrium that potentially triggers a series of hierarchical oxidative stress responses, changes in glutathione (GSH) levels were assessed in a luminescence-based GSH-Glo assay.[36] The results demonstrated that CNC-1, CNC-2, and CNC-3 significantly decreased the abiotic GSH levels to 78.98 ± 7.69%, 61.99 ± 6.19%, and 41.85 ± 7.18% of the control, respectively. Furthermore, CNC-3 induced significantly stronger GSH depletion than CNC-2 and CNC-1 ($p < 0.05$). However, CNF-1 or CNF-2 did not show any pronounced effect (Figure 1C). To ensure that the prepared nanocellulose was ruled out of bacterial contamination for biological experimentation, the use of a Limulus amebocyte lysate (LAL) assay was performed to detect the endotoxin levels of 25 μg/mL nanocellulose samples. The result in Figure S1 (Supporting Information) showed endotoxin levels < 0.5 EU/mL across the board.

2.2 Nanocellulose Induces Differential Cytotoxic Responses in KUP5 and Hepa 1−6 Cells

Cell viability studies were undertaken to obtain provisional toxicological profiling of the nanocellulose in transformed KC (KUP5) and hepatocyte (Hepa 1−6) cell lines.[27,37] Both the ATP and MTS results in Figure 2A demonstrated that there were differential response profiles as a reflection of nanocellulose length in both cell types over a dose range of 0–200 μg/mL and the ATP assay showed a more obvious difference possibly due to its higher sensitivity than that by MTS assay. While CNF-1 and CNF-2 failed to interfere in cell viability in these cell types, except for KUP5 cells at the highest dose of 200 μg/mL, all CNC samples (including CNC-1, CNC-2, and CNC-3) showed more significant toxicity in KUP5 cells than that in Hepa 1−6 cells. The toxicity of CNC samples in KUP5 cells was length- and dose-dependent and the CNC-2 sample exhibited significantly higher toxicity than CNC-1 and CNC-3, especially at a high concentration (≥ 100 μg/mL). Compared to KUP5 cells, Hepa 1–6 cells were less sensitive to the adverse effects of CNC samples and only CNC-2 induced significant toxicity in Hepa 1–6 cells. The heat maps in Figure 2B display the differential cytotoxicity response profiles using a one-way ANOVA statistical method, where yellow indicates significant toxicity, and the green represents the absence of toxicity. These results indicate different cytotoxic effects between CNC and CNF samples to the liver cell types and the toxicity of CNC samples was length- and cell type-dependent with CNC-2 showing a stronger effect in KUP5 cells.

It is interesting that CNC samples also induced significant morphological alteration in KUP5 cells, which showed the cell shrinkage and convolution as well as single cells or small clusters of cells (Figure 2C). This morphological change is similar to ZnO treatment, a positive control for apoptotic cell death as demonstrated previously,[35] suggesting an apoptotic cell death mechanism may be involved for CNCs. Thus we embarked on this study to elucidate the detailed mechanisms involved in CNC-induced cytotoxicity. The toxicity of nanoparticles in liver cells is majorly ascribed to the programmed cell death (or apoptosis) mediated by caspase-3/7 activation or the pyroptosis involved in the caspase-1 activation and giant cell blebbing formation.[27,28,37] To explain the toxicity induced by nanocellulose, further biological assays were carried out to explain the mechanisms of injury in relation to the length of nanocellulose, cellular uptake level, and cell type.

2.3 Nanocellulose-Induced Toxicity is Attributed to Caspase-3/7-Mediated Apoptosis

The results in Figure 1B–C showed that nanocellulose was capable to induce abiotic ROS, as a reflection of their redox-active service states. The cell death induced by CNC samples may result from the generation of cellular oxidative stress in the liver cells. The assessment of cellular oxidative stress generation was firstly performed in KUP5 cells, using confocal microscopy to detect MitoSOX red fluorescence intensity to determine mitochondrial ROS (mtROS) production (Figure 3A). While CNC-1, CNC-2, and CNC-3 could induce the dye oxidation in cells, similar to ZnO, the positive control, there was no effect by CNF-1 or CNF-2. Quantitative expression of the fluorescence intensity in a microplate reader confirmed that mtROS production in KUP5 cells, treated with CNC-1, CNC-2, and CNC-3, was significantly higher than treatment with similar CNF-1 or CNF-2 (Figure 3B). Interestingly, CNC-2 induced a stronger response than CNC-1 and CNC-3 ($p < 0.05$).

The generated oxidative stress is capable to trigger caspase-induced apoptotic cell death through the perturbation of mitochondrial PT pores.[37] Assessment of the specific cleavage of a fluorescent FAM-FLICA caspase-3/7 substrate was performed by confocal microscopy. The confocal images in Figure 3A demonstrate the robust protease activation by CNC-1, CNC-2, and CNC-3 but not CNF-1 or CNF-2 in KUP5 cells. Quantitative expression of the data, using a microplate reader, furtherly confirmed the confocal data (Figure 3C). These results demonstrated that CNC-2 induced a significantly stronger response than CNC-1 and CNC-3 ($p < 0.05$).

Assessment of the mechanism of cell death was also performed by Annexin V-FITC and propidium iodide (PI) staining. The flow cytometry analysis in Figure 3D demonstrated 37.5%, 55.0%, and 45.4% of KUP5 cells were stained with Annexin V after the exposure to CNC-1, CNC-2, and CNC-3, respectively, indicating the apoptotic cell death involved, including early apoptosis and late-stage apoptosis (Q1 and Q2). The dual Annexin V-FITC/PI staining (Q2) confirmed the appearance of 11.3%, 14.8%, and 9.4% apoptotic KUP5 cells during the exposure to CNC-1, CNC-2, and CNC-3, respectively. In contrast, CNF-1 or CNF-2 did not show significant evidence of apoptosis compared to CNC treatments although the longer CNFs would possibly degrade into shorter components and could slightly induce early apoptosis. These data are in agreement with mtROS production and caspase-3/7 activation, demonstrating the apoptosis in KUP5 cells after CNC exposure. Additionally, similar to the toxicity result, only CNC-2 induced significant mtROS generation (Figure 3E) and caspase-3/7 activation (Figure 3F) in Hepa 1–6 cells, indicating the toxicity induced by CNC-2 was ascribed to the apoptosis. Overall the toxicity in the liver cells induced by the nanocellulose could be attributed to caspase-3/7 mediated-apoptosis through mtROS generation.

2.4 Cellular Uptake Mechanisms Determine the Differential Nanocellulose Toxicity to KUP5 and Hepa 1–6 cells

The cytotoxicity induced by nanoparticles (NPs) is dependent on their physical interactions with the cell membrane. Knowledge about the mechanism for NP entry into cells and subsequent intracellular transport is important to understand the toxic mechanism of the NPs.[38,39] This is necessary to assess the subcellular localization of nanocellulose materials. To visualize the cellular uptake of nanocellulose (not viewable by TEM), we prepared CNC and CNF fluorescence labeling by covalent attachment of fluorescein isothiocyanate (FITC) to the carbon backbone, using amination and conjugation chemistry, as described previously.[15,40] The liver cells were incubated with 50 μg/mL FITC-labeled materials for 16 h and visualized under a confocal microscope. The cell membrane was counter-stained with Alexa Fluor 594-labeled WGA antibody (red) and the nucleus was stained with Hoechst 33342 dyes (blue). The confocal images in Figure 4A and Figure S2 showed the cellular uptake of CNCs *vs* CNFs and in KUP5 *vs* Hepa 1−6 cells; while the significant intracellular accumulation of CNCs was visualized inside cells and more CNC-2 was present inside of the cells than CNC-1 or CNC-3, most CNFs showed adsorption on the plasma membrane with limited cellular uptake. Additionally, more FITC-labeled CNCs were available in KUP5 cells compared to Hepa 1–6 cells, demonstrating cellular uptake of nanocellulose materials in KUP5 cells was significantly higher than those in Hepa 1–6 cells. This result is consistent with the cell type-dependent cytotoxicity of these nanocellulose samples. The various mechanisms for cellular uptake of nanocellulose may be involved in the difference between KUP5 and Hepa 1–6 cells. To confirm the hypothesis, KUP5 cells were firstly treated with a phagocytosis inhibitor wortmannin (WM), a macropinocytosis inhibitor Cytochalasin D (Cyto D), and a clathrin-dependent endocytosis inhibitor Pitstop 2 under an incubation time and concentration without triggering cytotoxicity (data not shown) before CNCs exposure. Quantification for the FITC labeled nanocellulose incorporation in KUP5 cells and inhibitor effects on the cellular uptake were performed by a microplate reader. As shown in Figure 4B, the fluorescent intensity of CNC-2 was significantly higher than CNC-1 and CNC-3; Also, WM significantly inhibited the uptake of CNCs, while Cyto D and Pitstop 2 could not inhibit CNC uptake, suggesting that KUP5 cells take up CNCs predominantly through phagocytosis. This is further confirmed by confocal images in Figure 4C, where demonstrated the reduced uptake of FITC-CNC-2 under WM treatment rather than Cyto

D or Pitstop 2 treatment. Furthermore, the mtROS generation and caspase-3/7 activation induced by CNCs were significantly inhibited by phagocytosis inhibitor WM (Figure S3), indicating the CNCs-induced apoptosis in KUP5 cells was mediated by the phagocytosis of CNCs. As for Hepa 1–6 cells, both the confocal images and quantified data by a microplate reader (Figure 4D–E) showed a significant reduction in uptake of FITC-CNC-2 by Pitstop 2-treated Hepa 1–6 cells, suggesting the expected clathrin-mediated endocytosis of CNC-2 by Hepa 1–6 cells.

2.5 Phagocytosis of Nanocellulose Determines Inflammasome Activation in KUP5 Cells through Lysosome Damage, Leading to Cathepsin B Release

CNCs could be phagocytized by KUP5 cells. The cellular uptake of CNCs in KUP5 cells may lead to lysosome damage and trigger cathepsin B release, inducing caspase-1 activation. In order to assess lysosome integrity, we used fluorescent microscopy to detect a Magic Red-labeled cathepsin B substrate in cells. These images in Figure S4A showed that the punctate staining pattern of the intact lysosomes in untreated KUP5 cells disappeared upon exposure to CNCs and La_2O_3, the positive control of pyroptosis induced by lysosomal damage.[27] This can be explained by cathepsin B release into the cytosol, followed by leakage from the cell.[27] However, the integrity of the lysosomes in KUP5 cells treated with CNF-1 and CNF-2 did not show any significant effect. This is further confirmed by a microplate reader to quantify fluorescent intensity, where CNC treatments significantly reduced cathepsin B intensity rather than CNF samples (Figure S4B).

The caspase-1 activation by nanocellulose in KUP5 cells was assessed by confocal microscopy to observe the cleavage of the substrate, FAM-YVAD-FMK. As demonstrated in Figure 5A, the activation of caspase-1 by CNCs exposure for 16 h significantly increased compared to the control, similar to the positive La_2O_3, while no significant effect was observed on the activation of caspase-1 by CNF-1 or CNF-2. The quantified data measured by a microplate reader confirmed the significant caspase-1 activation by CNC samples rather than CNF samples in KUP5 cells (Figure 5B) and CNC-2 demonstrated significantly stronger effects than CNC-1 or CNC-3 ($p < 0.05$). Furthermore, the caspase-1 activation by CNCs was significantly inhibited by NLRP3 inflammasome inhibitor MCC950 (Figure S5) and lysosome inhibitor Bafilomycin A1 (Baf A1) (Figure S6).

NLRP3 inflammasome and caspase-1 activation lead to cleavage of pro-IL-1β to mature IL-1β.[44] We assessed IL-1β release from KUP5 cells after nanocellulose treatments by enzyme-linked immunosorbent assay (ELISA). As shown in Figure 5C, the secretion of IL-1β in KUP5 cells treated by CNCs significantly increased compared to the control, similar to positive La_2O_3. The CNF-1 and CNF-2 were no significant effect on the production of IL-1β in KUP5 cells. These results were consistent with their cellular uptake, cathepsin B release, and caspase-1 activation in KUP5 cells. Furthermore, the IL-1β secretion induced by CNCs was significantly inhibited by lysosome inhibitor Baf A1, cathepsin B inhibitor CA-074-Me, and NLRP3 inflammasome inhibitor MCC950, respectively (Figure 5D). All considered these results indicated that phagocytosis of CNCs induced lysosome damage, cathepsin B release, triggering caspase-1 activation and IL-1β release in a cellular uptake-dependent manner, and CNC-2 that was much phagocytosed by

KUP5 cells showed stronger effects than CNC-1 or CNC-3. Additionally, the CNC exposure to KUP5 cells induced the length-dependent TNF-α production with CNC-2 showing more significant effects than CNC-1 or CNC-3, while CNFs did have any significant effect (Figure S7). This is furtherly confirmed the inflammatory responses induced by nanocellulose materials.

2.6 Dominant Caspase-3/7 Activation is Induced Earlier than Caspase-1

The induction of caspase-1 activation and IL-1β production in KUP5 cells is generally suggestive of a unique form of cell death known as pyroptosis, which is mediated by caspase-1 activation and the formation of surface membrane pores by N-terminal of GSDMD upon its cleavage by caspase-1.[45–47] The CNC-treated KUP5 cells demonstrated significant caspase-3/7 mediated-apoptotic morphological change, not the caspase-1 mediated-pyroptotic morphological change including cell swelling and surface blebbing. The crosstalk between caspase-1 and caspase-3/7 activation could be available and caspase-3/7 could block pyroptosis by cleavage of GSDMD at sites that differ from the proteolysis by inflammatory caspases (caspase-1, 4, and 5).[48] To prove the hypothesis, we compared the activities of caspase-3/7 and caspase-1 in KUP5 cells exposed CNCs for 5 h. The fluorescent images in Figure 6A demonstrated that caspase-3/7 activation in KUP5 cells treated with CNCs was available, similar to the positive control of ZnO and CNC-2 also demonstrated stronger effects than CNC-1 or CNC-3, while there was no activation of caspase-1 in KUP5 cells treated with CNCs for 5 h, differing from the positive control of La_2O_3. This is further confirmed by quantified data obtained from a microplate reader (Figure 6B–C). However, it was possible to demonstrate caspase-1 activation by CNCs after a longer incubation period of 16 h in KUP5 cells (Figure 3A), suggesting the time-dependent activation of caspase-1 and that was later than caspase-3/7 activation. These results indicate that CNCs are the robust inducers of caspase-3/7 in KUP5 cells in a length-dependent manner, where the activation of caspase-1 is delayed.

2.7 Correlation of Cellular Responses as a Function Length of Nanocellulose

The physicochemical properties of nanocellulose were found to highly link with their cellular responses.[49] To better understand the role of length in nanocellulose-induced adverse effects, we performed correlation studies by looking at cellular responses in KUP5 cells, e.g., cytotoxicity, mtROS generation, caspase-3/7 activation, caspase-1 activation, and IL-1β release, as a function nanocellulose physicochemical properties, including length, aspect ratio, zeta potential, abiotic ROS, and abiotic GSH. The results were represented as a heat map of coefficient of correlation (R^2) with the green color denoting higher and red color being lower or no correlation (Figure 7A). Compared to other physicochemical properties, the length and aspect ratio of nanocellulose displayed a significantly higher coefficient of determination (R^2) to all tested cellular responses. Further, the length of nanocellulose rather than its aspect ratio showed a much higher correlation with cellular responses in KUP5 cells, especially for caspase activation and IL-1β release. The correlation plots in Figure 7B–C furtherly confirmed the vital role of nanocellulose length in the toxic effects, where demonstrated the nanocellulose length was highly correlated with cytotoxicity ($R^2 = 0.957$) and showed higher R^2 with other cellular responses than aspect ratio ($R^2 > 0.45$). Interestingly, these results performed negative correlations, suggesting shorter nanocellulose materials will induce stronger cytotoxic responses with CNCs in the ~280 nm length (CNC-2) showing the most significant effects. Taken together, the length of nanocellulose played a vital role in the cytotoxic responses in KUP5 cells, which is more predominant than the aspect ratio of nanocellulose.

2.8 Nanocellulose Induces Length-Dependent Toxicity and Inflammatory Response in Other Macrophages

It is well known that the toxic effects induced by CNCs are cell-type dependent. To demonstrate the sensitivity of our results to other cell lines, a limited number of studies were performed in RAW 264.7 and J774A.1 cell lines (Figure 8). While treatment with CNC-1, CNC-2, and CNC-3 resulted in cell viability reduction in RAW 264.7 and J774A.1 cells, CNF-1 and CNF-2 failed to interfere in cell viability in these macrophages (Figure 8A–B). Also, CNC-2 showed significant toxic effects than CNC-1 and CNC-3 ($p < 0.05$). Additionally, CNC-treated RAW 264.7 and J774A.1 cells responded with increased IL-1β production. This also demonstrated a length-dependent effect with CNC-2 showing stronger responses and CNFs showing no significant effects (Figure 8C–D), consistent with the results in KUP5 cells. The cathepsin B inhibitor CA-074-Me also abrogated the IL-1β production by CNCs, indicating the vital role of cathepsin B-mediated inflammatory response in RAW 264.7 and J774A.1 cells. These data suggest the induction of length-dependent toxicity and inflammatory response in RAW 264.7, J774A.1, and KUP5 cells as a specific feature of phagocytic cells in response to nanocellulose materials.

3. Discussion

In this study, we determined the effects of nanocellulose with different lengths from ~150 to ~6700 nm, on two major liver cell types, KCs and hepatocytes. We demonstrated the length- and cell-type-dependent effects of nanocellulose on the cellular uptake, cellular responses, and cytotoxicity in KUP5 and Hepa 1–6 cells. While all the shorter nanocellulose materials (CNC-1, CNC-2, and CNC-3), especially the CNC-2, triggered significant cytotoxicity in KCs, only CNC-2 induced toxicity to hepatocytes, the longer nanocellulose materials (CNF-1 and CNF-2) did not induce significant toxicity to these cells due to their minimal cellular uptake, except for the highest dose of 200 μg/mL to KUP5 cells. For KCs, they took up more CNCs *via* phagocytosis, which induced mtROS generation, caspase-3/7 activation, and apoptotic cell death. Additionally, the phagocytosis of CNCs triggered lysosomal damage, cathepsin B release, caspase-1 activation, and IL-1β production without pyroptosis due to dominant caspase-3/7 activation that happened earlier than caspase-1 activation. For Hepa 1–6 cells, they only took up less CNC-2 with ~280 nm length and the mechanism involves clathrin-mediated endocytosis. The limited cellular uptake of CNC-2 also induced mtROS generation, caspase-3/7 activation, and subsequent apoptotic cell death in Hepa 1–6 cells. In this study, we showed the length of nanocellulose played a vital role in the toxicity and inflammatory responses in a cell type-dependent fashion, confirmed by the correlation analysis between physicochemical properties of nanocellulose and cellular responses. Moreover, the length-dependent toxicity and inflammatory response were confirmed using additional RAW 264.7 and J774A.1 cells, suggesting it is a universal feature for macrophages.

An important finding of the current study is the delineation of differential length-dependent cytotoxicity of nanocellulose in the major liver cell types, KCs and hepatocytes, depending on their cellular uptake. Generally, nanocellulose is considered to be biocompatible (no or low cytotoxicity), while recent studies reported that nanocellulose has been shown to exert toxic effects in tissue culture systems.[12–14] The nanocellulose effects on the liver, where biomedical use of nanocellulose as drug delivery carriers will be accumulated due to liver filtration function, has not been performed. We found that the shorter nanocellulose samples (including CNC-1, CNC-2, and CNC-3), not the longer nanocellulose samples (including CNF-1 and CNF-2), triggered significant cytotoxicity in KCs due to their differential cellular uptake; However, only CNC-2 induced slight toxicity in hepatocytes due to its less cellular uptake. Furthermore, the length of nanocellulose showed a highly negative correlation with cytotoxicity and other adverse effects including mtROS generation, caspase activation, and IL-1β production. Interestingly, the CNC-2 with ~280 nm length demonstrated stronger cytotoxicity or inflammatory responses due to its cellular uptake more than other lengths despite CNC-2 showed less intrinsic oxidative stress than CNC-3 with ~720 nm length (Figure 1B–C). This may because the ~280 nm nanocellulose could more readily pass through the cell membrane and entered into cells than other scales, due to less energy needed.[50] This result is also compatible with the recent demonstration that phagocytic processing of high aspect ratio nanomaterials by macrophages is dependent on length, aspect ratio, or contact angle with the 200–300 nm nanomaterials showing strong effects.[15,51–53] Although the previous study demonstrated the aspect ratio of nanocellulose determined their pro-inflammatory in THP-1 cells without significant cytotoxicity, the current study showed that length, not aspect ratio, was the most important parameter in the nanocellulose-induced cytotoxicity and inflammatory responses in KCs (Figure 7). Furthermore, the length-dependent toxic effects were confirmed by the RAW 264.7 and J774A.1 cell lines, indicating it is a universal feature in macrophages.

Another significant finding of this work is the identification and elucidation of the detailed toxicity mechanism of cell type-dependent apoptotic cell death induced by CNCs in the liver cells. CNCs could induce intrinsic oxidative stress, as demonstrated by abiotic ROS production and abiotic GSH depletion in Figure 1B–C. Nanocellulose can be taken up by cells and macrophages exhibits a higher uptake capacity than the non-phagocytic cells.[11] Further, the intracellular CNCs could induce adverse effects due to intracellular oxidative stress.[54] In addition to the reported inflammatory responses as reflected by the NLRP3 inflammasome activation through lysosome rupture and cathepsin B release as well as the IL-1β secretion,[11,15,47] the CNCs inside liver cells also induced mtROS generation and caspase- 3/7-mediated apoptosis in the current study. This is demonstrated by the qualitative confocal images (Figure 3A) and quantified data by a microplate reader and flow cytometry (Figure 3B–D). Also, a stronger effect was available in KCs than hepatocytes based on the different cellular uptake mechanism-mediated uptake levels of CNCs in these cell lines. For KCs, they took up more CNCs through phagocytosis while hepatocytes only took up less CNC-2 through clathrin-mediated endocytosis, as confirmed by the treatments with various inhibitors including a phagocytosis inhibitor WM, a clathrin-dependent endocytosis inhibitor Pitstop 2, or a macropinocytosis inhibitor Cyto D.[28,55,56] The differential cellular response depending on the CNC uptake mechanism was also supported by our previous studies to determine the toxic effects of GO and molybdenum disulfide (MoS_2) nanoparticles on the liver cells.[28,57]

In our previous studies, the phagocytosis of REO and GO nanoparticles induced NLRP3 inflammasome activation in KUP5 cells, which further induced the GSDMD-mediated pyroptotic cell death, characterized by cell swelling and surface blebbing.[28,45,58] However, the pyroptotic morphological change was not observed after CNC exposure despite caspase-1 activation and inflammatory response induction. In contrast, the CNC exposure induced significant apoptotic cell death in KUP5 cells, similar to the positive control of ZnO treatment. We posit that the early (≈5 h) activation of caspase-3/7 triggered apoptosis and cleaved GSDMD at an alternative cleavage site that interfered with the generation of pore-forming N-terminal GSDMD fragments by caspase-1 and the subsequent pyroptotic cell death.[47,48] This is also in keeping with reported experimental studies, demonstrating that MoS_2 and V_2O_5 nanoparticles induced caspase-1 activation without triggering pyroptosis in KUP5 cells.[37,57]

What lessons can be drawn from our results about knowledge of nanocellulose safety? We extend the observations of significant cytotoxicity and inflammation induced by nanocellulose, which is related to differences in the cellular uptake of CNCs *vs* CNFs, [11] by providing structure-activity relationships, demonstrating the importance of length and cell type that underpin toxic and pro-inflammatory effects in liver cells. The shorter nanocellulose samples (CNCs) can induce stronger apoptotic cell death than longer nanocellulose samples (CNFs) and the CNC with ~280 nm length (CNC-2) showed the most significant toxic responses due to higher cellular uptake. Our findings provide useful information to evaluate nanocellulose effects and design safer nanocellulose materials for biomedical applications. This study is mainly an *in vitro* proof-of-principle study to elucidate the impact of nanocellulose with different lengths on the major liver cell types including KCs and hepatocytes, and it should not be construed as liver toxicity *in vivo* because nanocellulose will require further surface modifications (e.g., pegylation) to improve dispersibility and stability in the physiological media and reduce clearance by the MPS for biomedical applications. Currently, there is a lack of direct evidence of the nanocellulose-induced cell death in the liver *in vivo*. However, a recent study showed that the nanocellulose modified with oxalate ester has been reported to induce the potential hepatotoxicity *via* the inflammation-related iNOS and apoptosis-related Bax protein expression in the liver of rats,[20] which is consistent with our results. Further *in vivo* studies will be necessary to demonstrate nanocellulose-induced toxicity to the liver in a cell type-specific fashion.

4. Conclusions

In this study, we demonstrate the length- and cell-type-dependent toxic effects of nanocellulose on the major liver cell types, KCs and hepatocytes. While all the shorter nanocellulose samples (CNCs), especially the CNC-2, triggered significant cytotoxicity in KCs, only CNC-2 induced slight toxicity to hepatocytes, the longer nanocellulose samples (CNFs) did not induce significant toxicity to these cells. The differential toxicity is due to their cellular uptake levels, mediated by the uptake mechanism of cells, and CNC-2 induced the highest level of uptake. The phagocytosis of CNCs by KCs induced mtROS generation, caspase-3/7 activation, and apoptotic cell death. In addition, the phagocytosed CNCs could also trigger lysosomal damage, cathepsin B release, NLRP3 inflammasome and caspase-1 activation, leading to IL-1β production without evidence of pyroptotic morphological changes. The cellular uptake of CNC-2 by Hepa 1–6 cells was through clathrin-mediated endocytosis, which induced mtROS generation and caspase-3/7-mediated apoptotic cell death. Compared to other physicochemical prosperities, the length of nanocellulose showed the highest correlation in cell type-dependent toxicity and inflammatory responses, which is a universal feature as demonstrated in other macrophage cell lines. Overall this study elucidated the mechanism of differential toxicity of nanocellulose on liver cells, which provided valuable information on the safety profiles of nanocellulose on the liver for their potential biomedical applications.

5. Experimental Section

Materials:

Various nanocellulose samples with different lengths were provided by Engineered Nanomaterials Resource and Coordination Core, part of NHIR Consortium of the NIEHS. The transformed mouse Kupffer cell line, KUP5, was purchased from RIKEN Cell Bank (Japan). The other mouse macrophage cell lines, including RAW 264.7 and J774A.1 cells, were purchased from Sigma (St. Louis, MO). The mouse hepatocyte cell line, Hepa 1−6, was purchased from ATCC. The fetal bovine serum (FBS) was purchased from Gemini Bio-Products (West Sacramento, CA). The penicillin-streptomycin (PS) was purchased from Gibco (Waltham, MA). The CellTiter 96 aqueous one solution cell proliferation assay (MTS) and GSH-Glo glutathione assay kits were purchased from Promega (Madison, WI). The ATPlite 1step Luminescence Assay kit was purchased from PerkinElmer Inc. (Waltham, MA). The Hoechst 33342 and Alexa Fluor 594-conjugated wheat germ agglutinin (WGA) were purchased from Life Technologies (Grand Island, NY). MitoSOX indicator and 2′,7′-dichlorodihydrofluorescein diacetate (H_2DCFDA) were purchased from Invitrogen (Carlsbad, CA). The FITC (90%) was purchased from ACROS Organics™ (Fair Lawn, NJ). The FAM-FLICA Caspase-1, Caspase-3/7, and Magic Red Cathepsin B assay kits were purchased from ImmunoChemistry Technologies, LLC (Bloomington, MN). The LPS, WM, Cyto D, Pitstop 2, Baf A1, CA-074-Me, and MCC950 were purchased from Sigma (St. Louis, MO). The ELISA kits for mouse IL-1β and TNF-α were purchased from R&D Systems (Minneapolis, MN).

Physicochemical Characterizations of Nanocellulose:

The 5 mg/mL of stock suspensions of CNCs and CNFs in DI water were prepared by vortexing and bath sonication for 15 min in a water bath sonicator (Branson 2510) with 100 W output power and 42 kHz frequency. The work solutions were prepared by diluting these stock suspensions with DI water and further used for the physicochemical characterization to determine primary length and diameter, using TEM (JEOL 1200 EX) at an accelerating voltage of 80 kV. It was performed by placing a drop of the 50 μg/mL of suspension in DI water on a 400 mesh Cu TEM grid, followed by evaporation at room temperature. The samples were negatively stained with 2 wt% uranyl acetate solution before TEM viewing.

The assessments of hydrodynamic size and surface charge of the nanocellulose samples at 50 μg/mL in DI water or DMEM medium were performed by a ZetaPALS particle sizer and zeta potential analyzer (Brookhaven Instruments, Holtsville, NY). The evaluation of endotoxin levels of nanocellulose samples was performed using a Limulus amebocyte lysate (LAL) assay (Lonza, Walkersville, MD) according to the manufacturer’s procedure.[15]

Assessing the Intrinsic Oxidative Potential of Nanocellulose:

The abiotic ROS generation by nanocellulose was detected by H_2DCFDA fluorescence.[34] The DCF working solution was prepared by a dissolve of 50 μg H_2DCFDA in 17.3 μL ethanol, followed by the addition of 692 μL of a 0.01 mol/L sodium hydroxide solution and incubation for 30 min. Then, 3500 μL of a sodium phosphate buffer (pH 7.4, 25 mmol/L) was added to form a 29 μmol/L DCF solution. After this, 80 μL/well DCF work solution was added to a 96 multiwell black plate (Costar, Corning, NY), followed by the addition of a 20 μL of 200 μg/mL nanocellulose suspension to each well for 2 h incubation. The DCF fluorescence emission spectra in the range of 500–600 nm at an excitation wavelength of 490 nm were collected using a SpectraMax M5e microplate reader (Molecular Devices, Sunnyvale, CA). The treatment with ZnO nanoparticles was used as a positive control.

The GSH-Glo glutathione assay, a luminescence-based assay for detecting and quantifying GSH based on the conversion of a luciferin derivative to luciferin by glutathione S-transferase (GST), was used to assess the effect on abiotic redox equilibrium by nanocellulose according to the manufacturer’s procedure.[36] Briefly, 10 μL of nanocellulose at 200 μg/mL was added to a 96-well white plate (Costar, Corning, NY), followed by the addition of 90 μL of GSH-Glo agent for 30 min. Then, it was added the 100 μL of luciferin detection agent to each well, followed by detecting the luminescence by a SpectraMax M5e microplate reader. The treatment with ZnO nanoparticles was used as a positive control.

Cell Culture:

KUP5 cells were cultured in high-glucose DMEM with the supplement of 10% FBS, 250 μM 1-thioglycerol, 100 U/mL to 100 μg/mL of PS, and 10 μg/mL bovine insulin. Hepa 1–6, RAW 264.7, and J774A.1 cells were cultured in a high-glucose DMEM medium, supplemented with 10% FBS and 100 U/mL to 100 μg/mL PS.

Determination of Nanocellulose Cytotoxicity:

The cell viability of these cell lines was performed using the MTS or ATP assay, respectively. Cells, seeded at a density of approximately 3 × 10^4/well in 96-well plates, were exposed to nanocellulose samples at the concentrations of 0–200 μg/mL for 24 h in a humidified 5% CO_2 incubator, respectively. The cell culture media were removed and replaced with 100 μL of complete culture media containing 16.7% MTS stock solution for 0.5 h. To spin down the cell debris and nanocellulose samples, these plates were centrifuged by an Eppendorf 5430 microcentrifuge at 2000 rpm for 10 min. Then, an 80 μL amount of the supernatant was collected from each well, followed by transferring into a new 96-well plate to detect the absorbance of formed formazan at 490 nm on a microplate reader. Also, cell viability was accessed by the ATPlite 1step assay to determine the cellular ATP content according to the manufacturer’s instructions. The luminescence intensity was read on a

SpectraMax M5 microplate reader. The control cells without any treatment (0 μg/mL) were considered to display 100% cell viability, according to which the viability of the treated cells was adjusted. The ZnO treatment was used as a positive control.

Assessment of Cell Morphology Change under Optical Microscopy:

KUP5 and Hepa 1–6 cells were exposed to 50 μg/mL nanocellulose samples for 16 h in a 12-well plate, respectively. The morphology of the cell was monitored using a Zeiss Optical Microscope (Oberkochen, Germany) and compared with the ZnO treatment, the positive control of apoptotic cell death.

Determination of mtROS Generation by Nanocellulose:

KUP5 and Hepa 1–6 cells, seeded at approximately 1 × 10^5 cells/well in an 8-well Lab-Tek chamber slide and exposed to 50 μg/mL of nanocellulose samples for 16 h, were washed with PBS three times and treated with 5 μM MitoSOX in HBSS at 37 °C for 10 min. Then, these cells were stained with 5 μg/mL Hoechst 33342 for 15 min and imaged using a Leica Confocal SP8-SMD microscope (Leica, Germany). The quantification for fluorescence intensity in the cells was obtained by a SpectraMax M5 microplate reader at excitation/emission wavelengths of 510/580 nm. The ZnO treatment was used as a positive control.

Determination of the Activations of Caspase-3/7 and Caspase-1:

KUP5 and Hepa 1–6 cells, seeded at approximately 1 × 10^5 cells/well in an 8-well Lab-Tek chamber slide, were incubated with 50 μg/mL of nanocellulose samples, respectively. The treated cells were washed in PBS three times and stained with FAM-FLICA Caspase-3/7 or Caspase-1 substrates at 37 °C for 1 h according to the manufacturer's procedures. After this, these cells were stained with Hoechst 33342 for 15 min and imaged by a confocal microscope. The quantification for fluorescence intensity in the cells was obtained by a microplate reader at excitation/emission wavelengths of 492/520 nm. The treatment with ZnO nanoparticles was used as a positive control for caspase-3/7 activation. The treatment with La_2O_3 nanoparticles was used as a positive control for caspase-1 activation.[27]

Determination of Apoptosis via Annexin V-FITC/PI Staining and Flow Cytometry:

KUP5 cells, plated at a density of approximately 6 × 10^5 cells/well in a 6-well plate, were primed by 1 μg/mL of LPS for 4 h and then incubated with 50 μg/mL of nanocellulose suspensions containing 0.1 μg/mL LPS for 16 h. After the collection of the cell pellets washed with PBS three times, the cellular staining was performed by an Annexin V-FITC Apoptosis Detection Kit according to the manufacturer's introduction. The detection of Annexin V-FITC and PI staining in cells were performed with a BD LSR II Flow Cytometer by using FITC and PE channels, respectively. The Annexin V-FITC/PI-positive cells were identified as apoptotic populations and Annexin V-positive/PI-negative positive cells were identified as populations undergoing early apoptotic cell death.

Assessment of FITC-Nanocellulose Cellular Uptake through Confocal Microscopy and Microplate Reader:

FITC labeled cellulose was prepared by covalent attachment of FITC to the carbon backbone, using amination and conjugation chemistry as described before.[15,40] Briefly, 4.5 mL of the nanocellulose suspension (containing 50 mg of material) was transferred into a glass flask and added 500 μL of a 10 M NaOH solution while stirring, followed by the addition of 80 μL of epichlorohydrin (AR, Sigma) into the mixture with an increased temperature to 60 °C for 1.5 h. After cooling and centrifuging, the epoxy-activated nanocellulose pellet was dispersed and transferred into a glass flask, followed by adding 250 μL of an ammonium hydroxide solution (NH_4OH, 28–30 wt%, Sigma) while stirring at 60 °C for 3 h. The aminated nanocellulose ($CNC–NH_2$) was obtained for conjugation to FITC and the FITC-labeled nanocellulose was stored at 4 °C for further use.

To assess the cellular localization of nanocellulose, the KUP5 and Hepa 1–6 cells were exposed to 50 μg/mL of FITC-labeled nanocellulose suspensions for 16 h and washed by PBS three times. Cell membranes and nuclei were stained with 5 μg/mL of WGA and 8 μM of Hoechst 33342 for 15 min, respectively, followed by visualizing under a confocal microscope. To determine the cellular uptake mechanism of nanocellulose in KUP5 and Hepa 1–6 cells, before nanocellulose exposure, the cells were treated with various inhibitors including 1 μM WM for 0.5 h, 20 μM Pitstop 2 for 0.5 h, or 5 μg/mL Cyto D for 1 h, respectively.[28] The localization of nanocellulose in cells was visualized by a confocal microscope. To quantify the FITC-nanocellulose association with cells in the presence of inhibitors, KUP5 and Hepa 1–6 cells, seeded at a density of approximately 4×10^4/well in 96-well black plates, were incubated with various inhibitors and FITC-nanocellulose, respectively. The fluorescence intensity of FITC was measured by SpectraMax M5e microplate reader with an emission wavelength at 520 nm and an excitation wavelength at 494 nm. The control cells were treated with FITC-nanocellulose without inhibitors for comparison.

Assessment of Lysosomal Damage by Cathepsin B Staining:

KUP5 cells primed with LPS (1 μg/mL) for 4 h were exposed to 50 μg/mL of nanocellulose suspensions containing 0.1 μg/mL LPS for 16 h, followed by washing with PBS three times and incubating with the work solution of Magic Red Cathepsin B assay kit for 30 min according to the manufacturer’s protocol. Then, these cells were washed with PBS, stained with 5 μg/mL of Hoechst 33342 for 15 min, and imaged under a fluorescent microscope. The quantification for fluorescence intensity in the cells was monitored at excitation/emission wavelengths of 592/628 nm by a microplate reader. The treatment of L_2O_3 was used as a positive control.

Determination of IL-1β and TNF-α Release:

KUP5 cells primed with 1 μg/mL LPS for 4 h were exposed to 50 μg/mL of nanocellulose suspensions containing 0.1 μg/mL LPS for 24 h. The cellular supernatants were collected to quantify the levels of IL-1β and TNF-α by ELISA according to the manufacturer’s instructions, respectively. The treatment with La_2O_3 nanoparticles was used as a positive control.[36] The determinations of IL-1β release under treatment with various inhibitors, including V-ATPase inhibitor Baf A1 (100 nM for 0.5 h),[41] cathepsin B inhibitor CA-074-Me (30 µM for 6 h),[42] and NLRP3 inflammasome inhibitor MCC950 (10 µM for 0.5 h),[43] were performed to compare effects of inhibitors.

Statistical Analysis:

A two-tailed Student's t-test for two-group analysis or one-way ANOVA for multiple group comparisons were used in the current statistical analysis. All the values were expressed as the mean and standard deviation of three independent experiments (n = 3). A *p*-value of less than 0.05 was considered statistically significant.

Supplementary Material

Refer to Web version on PubMed Central for supplementary material.

Acknowledgments

Research reported in this publication was supported by the National Institute of Environmental Health Sciences of the National Institutes of Health under Award Number (U01ES027237) as part of the Nanotechnology Health Implications Research (NHIR) Consortium. The content is solely the responsibility of the authors and does not necessarily represent the official views of the National Institutes of Health. The engineered nanomaterials used in the research presented in this publication have been procured/developed, characterized, and provided by the Engineered Nanomaterials Resource and Coordination Core established at Harvard T. H. Chan School of Public Health (NIH grant # U24ES026946). The authors thank the CNSI Advanced Light Microscopy/Spectroscopy and Electron Imaging Center for NanoMachines Core Facilities and the Flow Cytometry Core Facility of Jonsson Comprehensive Cancer Center at UCLA.

References

[1]. Dufresne A, Mater. Today2013, 16, 220.
[2]. Wang X, Xia Q, Jing S, Li C, Chen Q, Chen B, Pang Z, Jiang B, Gan W, Chen G, Cui M, Hu L, Li T, Small2021, 17, e202008011.
[3]. Thomas B, Raj MC, Athira KB, Rubiyah MH, Sanchez C, Chem. Rev. 2018, 118, 11575. [PubMed: 30403346]
[4]. Salimi S, Sotudeh-Gharebagh R, Zarghami R, Chan SY, Yuen KH, ACS Sustain. Chem. Eng. 2019, 7, 15800.
[5]. Dao HNA, Leo CP, Environ. Res. 2021, 111100. [PubMed: 33812871]
[6]. Moon RJ, Martini A, Nairn J, Simonsen J, Youngblood J, Chem. Soc. Rev. 2011, 40, 3941. [PubMed: 21566801]
[7]. Li Q, Wu Y, Fang R, Lei C, Li Y, Li B, Pei Y, Luo X, Liu S, Trends Food Sci. Tech. 2021, 110, 573.
[8]. Ahankari S, Paliwal P, Subhedar A, Kargarzadeh H, ACS Nano2021, 15, 3849. [PubMed: 33710860]
[9]. Hasan N, Rahman L, Kim SH, Cao J, Arjuna A, Lallo S, Jhun BH, Yoo JW, J. Pharm. Investig. 2020, 50, 1.
[10]. Li F, Mascheroni E, Piergiovanni L, Packag. Technol. Sci. 2015, 28, 475.
[11]. Ventura C, Pinto F, Loureno AF, Ferreira P, Silva MJ, Cellulose2020, 27, 5509.
[12]. Lin N, Dufresne A, Eur. Polym. J. 2014, 59, 302.
[13]. Adamis Z, Tátrai E, Honma K, Ungváry G, J Appl. Toxicol. 2015, 17, 137.
[14]. Stoudmann N, Schmutz M, Hirsch C, Nowack B, Som C, Nanotoxicology2020, 14, 1241. [PubMed: 32909499]
[15]. Wang X, Chang CH, Jiang J, Liu Q, Liao YP, Lu J, Li L, Liu X, Kim J, Ahmed A, Nel AE, Xia T, Small2019, 15, e1901642. [PubMed: 31461215]

[16]. Yanamala N, Farcas MT, Hatfield MK, Kisin ER, Kagan VE, Geraci CL, Shvedova AA, ACS Sustain. Chem. Eng. 2013, 2, 1691.

[17]. Reinholz J, Landfester K, Mailander V, Drug Deliv. 2018, 25, 1694. [PubMed: 30394120]

[18]. Tsoi KM, Macparland SA, Ma X, Spetzler VN, Echeverri J, Ouyang B, Fadel SM, Sykes EA, Goldaracena N, Kaths JM, Conneely JB, Alman BA, Selzner M, Ostrowski MA, Adeyi OA, Zilman A, Mcgilvray ID, Chan WCW, Nat. Mater. 2016, 15, 1212. [PubMed: 27525571]

[19]. Roy P, Das S, Auddy RG, Saha A, Mukherjee A, Pharm Res2013, 30, 1252. [PubMed: 23319171]

[20]. Otuechere CA, Adewuyi A, Adebayo OL, Ebigwei IA, Hum. Exp. Toxicol. 2019, 39, 1538216903.

[21]. Zhang YN, Poon W, Tavares AJ, Mcgilvray ID, Chan WCW, Control J. Release2016, 240, 332.

[22]. Dixon LJ, Barnes M, Tang H, Pritchard MT, Nagy LE, Compr. Physiol. 2013, 3, 785. [PubMed: 23720329]

[23]. Bilzer M, Roggel F, Gerbes AL, Liver Int. 2006, 26, 1175. [PubMed: 17105582]

[24]. Hume DA, Curr. Opin. Immunol. 2006, 18, 49. [PubMed: 16338128]

[25]. Tsoi KM, Macparland SA, Ma XZ, Spetzler VN, Echeverri J, Ouyang B, Fadel SM, Sykes EA, Goldaracena N, Kaths JM, Nat. Mater. 2016, 15, 1212. [PubMed: 27525571]

[26]. Boey A, Ho HK, Small2020, 16, e2000153. [PubMed: 32163668]

[27]. Mirshafiee V, Sun B, Chang CH, Liao Y, Jiang W, Jiang J, Liu X, Wang X, Xia T, Nel AE, ACS Nano2018, 12, 3836. [PubMed: 29543433]

[28]. Li J, Wang X, Mei K, Chang CH, Jiang J, Liu X, Liu Q, Guiney LM, Hersam MC, Liao Y, Meng H, Xia T, Nano Today2021, 37, 1010161.

[29]. Gissen P, Arias IM, J. Hepatol. 2015, 63, 1023. [PubMed: 26116792]

[30]. Yi-Nan Zhang, Wilson Poon, Anthony J, Tavares Ian, Mcgilvray D, J. Control. Release2016.

[31]. Linares J, Matesanz MC, Vila M, Feito MJ, Gonçalves G, Vallet-Regí M, Marques PAAP, Portolés MT, ACS Appl. Mater. Inter. 2014, 6, 13697.

[32]. Kovacs T, Naish V, O’Connor B, Blaise C, Martel P, Nanotoxicology2010, 4, 255. [PubMed: 20795908]

[33]. Bhattacharya M, Malinen MM, Lauren P, Lou YR, Kuisma SW, Kanninen L, Lille M, Orlu AC, Guguen-Guillouzo C, Ikkala O, Control J. Release2012, 164, 291.

[34]. Zhang H, Pokhrel S, Ji Z, Meng H, Wang X, Lin S, Chang CH, Li L, Li R, Sun B, Wang M, Liao YP, Liu R, Xia T, Madler L, Nel AE, J. Am. Chem. Soc. 2014, 136, 6406. [PubMed: 24673286]

[35]. Tian X, Michael K, Monty L, Lutz M, Benjamin G, Haibin S, Joanne I Y, Jeffrey I Z, Andre E N, ACS Nano2008, 2, 2121. [PubMed: 19206459]

[36]. Li R, Guiney LM, Chang CH, Mansukhani ND, Ji Z, Wang X, Liao Y, Jiang W, Sun B, Hersam MC, Nel AE, Xia T, ACS Nano2018, 12, 1390. [PubMed: 29328670]

[37]. Wang X, Chang CH, Jiang J, Liu X, Li J, Liu Q, Liao YP, Li L, Nel AE, Xia T, Small2020, e2000528. [PubMed: 32337854]

[38]. Zhang B, Wei P, Zhou Z, Wei T, Adv. Drug Deliver. Rev. 2016, 105, 145.

[39]. Albanese A, Tang PS, Chan W, Annu. Rev. Biomed. Eng. 2012, 14, 1. [PubMed: 22524388]

[40]. Dong S, Roman M, J. Am. Chem. Soc. 2007, 129, 13810. [PubMed: 17949004]

[41]. Mauvezin C, Neufeld TP, Autophagy2015, 11, 1437. [PubMed: 26156798]

[42]. Hentze H, Lin XY, Choi M, Porter AG, Cell Death Differ. 2003, 10, 956. [PubMed: 12934070]

[43]. Tapia-Abellán A, Angosto-Bazarra D, Martínez-Banaclocha H, Torre-Minguela CD, Pelegrin P, Nat. Chem. Biol. 2019, 15, 560. [PubMed: 31086329]

[44]. He Y, Hara H, Núñez G, Trends Biochem. Sci. 2016, 41, 1012. [PubMed: 27669650]

[45]. Liu X, Zhang Z, Ruan J, Pan Y, Magupalli VG, Wu H, Lieberman J, Nature2016, 535, 153. [PubMed: 27383986]

[46]. Bergsbaken T, Fink SL, Cookson BT, Nat. Rev. Microbiol. 2009, 7, 99. [PubMed: 19148178]

[47]. Man SM, Karki R, Kanneganti T, Immunol. Rev. 2017, 277, 61. [PubMed: 28462526]

[48]. Taabazuing CY, Okondo MC, Bachovchin DA, Cell Chem Biol2017, 24, 507. [PubMed: 28392147]

[49]. Liu Y, Workalemahu B, Jiang X, Small2017, 13, 1701815.

[50]. Ma J, Liu R, Wang X, Liu Q, Chen Y, Valle RP, Zuo YY, Xia T, Liu S, ACS Nano2015, 9, 10498. [PubMed: 26389709]

[51]. Shang L, Nienhaus K, Nienhaus GU, J. Nanobiotechnol. 2014, 12, 5.

[52]. Champion JA, Mitragotri S, Proc. Natl. Acad. Sci. U.S.A2006, 103, 4930. [PubMed: 16549762]

[53]. Richards DM, Endres RG, Proc. Natl. Acad. Sci. U.S.A2016, 22, 6113.

[54]. Menas AL, Yanamala N, Farcas MT, Russo M, Friend S, Fournier PM, Star A, Iavicoli I, Shurin GV, Vogel UB, Chemosphere2017, 171, 671. [PubMed: 28061425]

[55]. von Kleist L, Stahlschmidt W, Bulut H, Gromova K, Puchkov D, Robertson MJ, Macgregor KA, Tomilin N, Pechstein A, Chau N, Chircop M, Sakoff J, von Kries JP, Saenger W, Krausslich HG, Shupliakov O, Robinson PJ, Mccluskey A, Haucke V, Cell2011, 146, 471. [PubMed: 21816279]

[56]. Mu Q, Su G, Li L, Gilbertson BO, Yu LH, Zhang Q, Sun Y, Yan B, ACS Appl. Mater. Inter. 2012, 4, 2259.

[57]. Li J, Guiney LM, Downing JR, Wang X, Chang CH, Jiang J, Liu Q, Liu X, Mei K, Liao Y, Ma T, Meng H, Hersam MC, Nel AE, Xia T, Small2021, 17, e202101084.

[58]. Fink SL, Cookson BT, Infect. Immun. 2005, 73, 1907. [PubMed: 15784530]

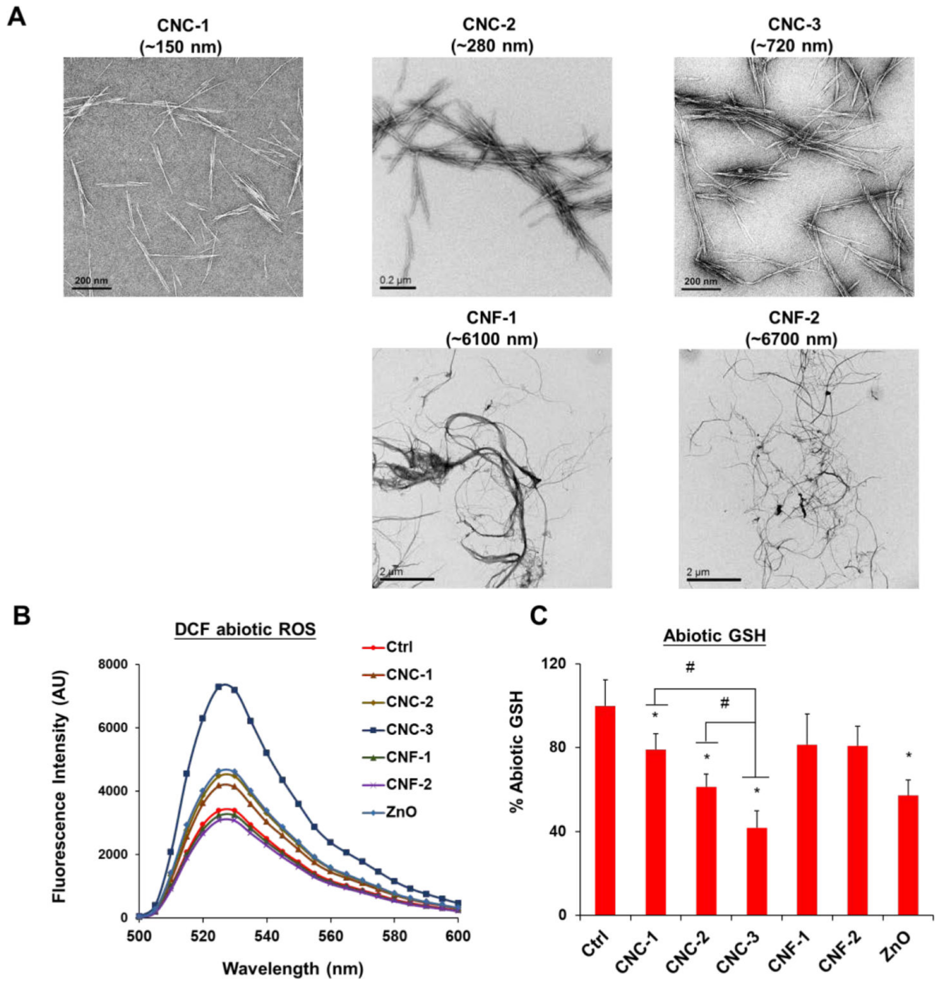

Figure 1. Physicochemical characterization of materials in the nanocellulose library.

(A) Representative of TEM images of CNC-1, CNC-2, CNC-3, CNF-1, and CNF-2 samples obtained by a JEOL 1200-EX TEM with an accelerating voltage of 80 K eV. The scale bar in CNC-1, CNC-2, and CNC-3 is 0.2 μm and in CNF-1 and CNF-2 is 2 μm, respectively. (B) H_2DCFDA fluorescence spectroscopy obtained by a SpectraMax M5e microplate reader under an excitation wavelength of 490 nm to demonstrate the abiotic ROS generation by CNC-1, CNC-2, CNC-3, CNF-1, and CNF-2, respectively. The ZnO nanoparticle treatment was used as a positive control. (C) Determination of the abiotic GSH content using the GSH-Glo agent. The luminescence was detected in the microplate reader, after the addition of 10 μL nanocellulose at 200 μg/mL to 90 μL of the GSH-Glo agent. The asterisk (*) represents a p-value < 0.05 compared to the control; # represents a p-value < 0.05 compared to the CNC-1 or CNC-2 treatment.

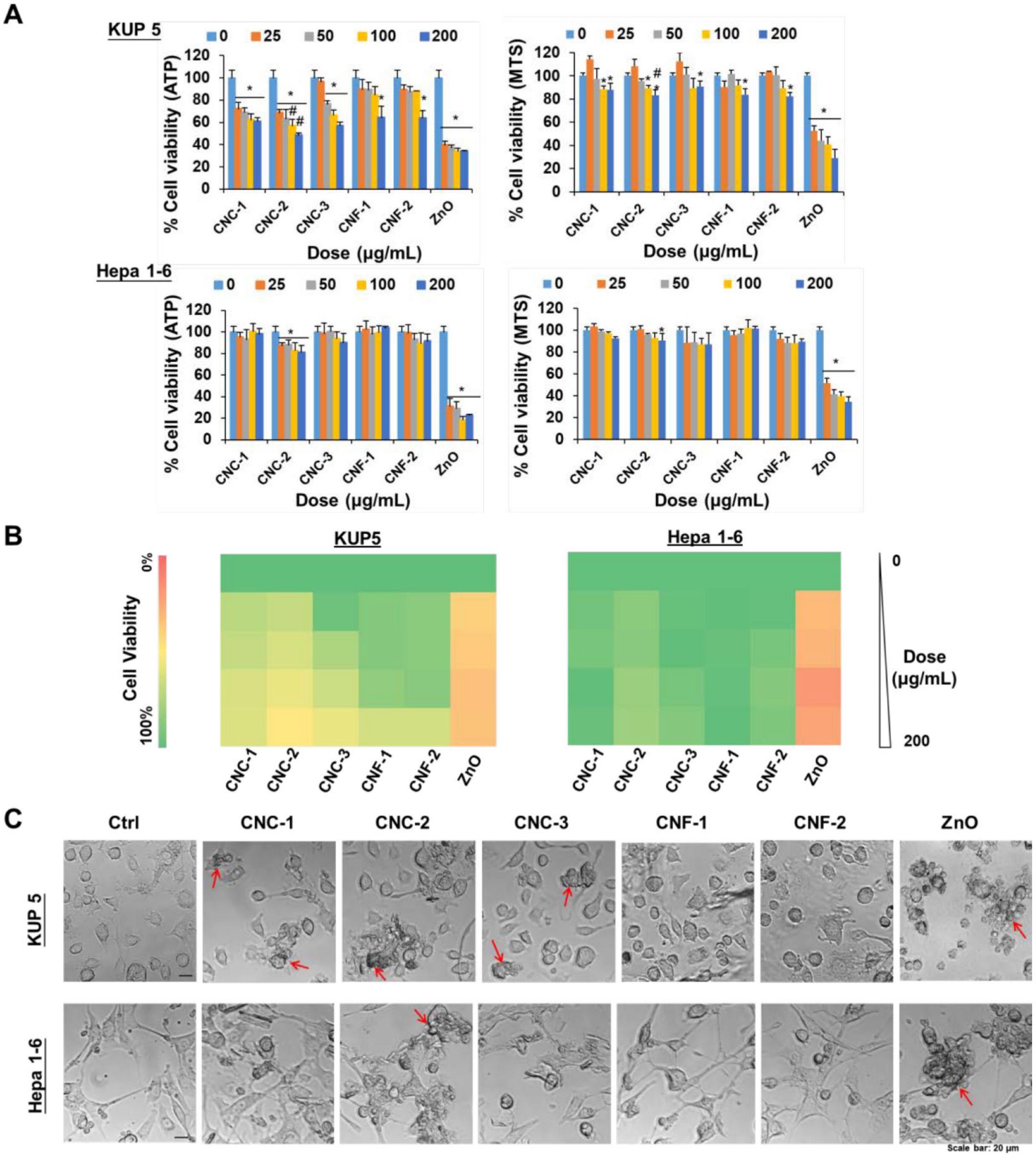

Figure 2. Assessment of nanocellulose cytotoxicity in KUP5 and Hepa 1–6 cells.

(A) Cell viability of KUP5 and Hepa 1–6 cells after exposure to nanocellulose at 0−200 μg/mL for 24 h, determined by ATP and MTS assay, respectively. The viability of untreated cells was set as 100%. The ZnO nanoparticle treatment served as a positive control. * represents a *p*-value < 0.05 compared to the untreated cells, while # represents a *p*-value < 0.05 for the comparison of CNC-2 with CNC-1 and CNC-3 treatment. (B) Heatmap to demonstrate the comparative toxicological impact on KUP5 and Hepa 1−6 cells following the color scale in the sidebar on the left. (C) Optical microscopy images to demonstrate cell morphologic changes in KUP5 and Hepa 1–6 cells, exposed to 50 μg/mL of nanocellulose samples for 24 h. The red arrows indicated the cell shrinkage and convolution as well as single cells or small clusters of cells, similar to the positive control of ZnO treatment. The scale bar in the image represents 20 μm.

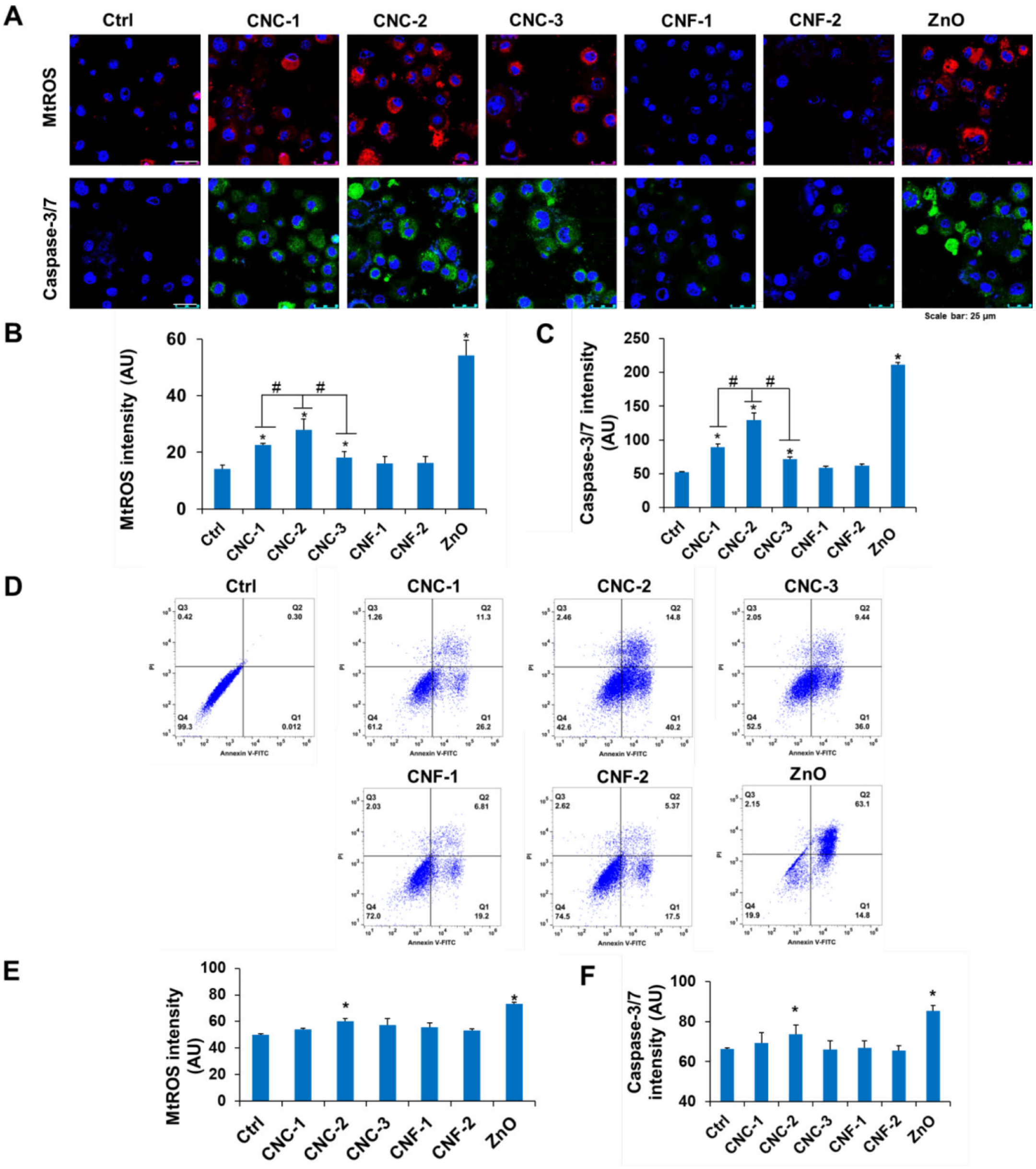

Figure 3. Determination of apoptotic cell death in the liver cells.

(A) Confocal images to determine mtROS generation (the upper line) and caspase-3/7 activation (the lower line) by nanocellulose in KUP5 cells. Cells were exposed to 50 μg/mL of the materials for 16 h, before staining with 5 μM red MitoSOX for 10 min in HBSS or the FAM-FLICA caspase-3/7 substrate (green) for 1 h, followed by staining with Hoechst 33342 (blue) for 15 min. ZnO treatment served as a positive control. The scale bar represents 25 μm. (B) Quantification of mtROS generation in KUP5 cells in a microplate reader. The fluorescence intensity was detected at excitation/emission wavelengths of 510/580 nm. * represents a $p < 0.05$ compared to the untreated control; # represents a p-value < 0.05 for the comparison of CNC-2 with CNC-1 and CNC-3 treatment. (C) Quantification of caspase-3/7 activation in KUP5 cells using a microplate reader. The fluorescence intensity was monitored at excitation/emission wavelengths of

492/520 nm. (D) Flow cytometry analysis to determine apoptotic KUP5 cells using dual Annexin V-FITC and PI staining. The primed KUP5 cells with 1 μg/mL lipopolysaccharide (LPS) for 4 h were treated with 50 μg/mL nanocellulose samples for 16 h, respectively. After washing, the cells were stained with the Annexin V-FITC Apoptosis Detection Kit according to the manufacturer's procedure. The Annexin V-FITC/PI-positive (Q2) cells were regarded as apoptotic populations. (E) Quantification of mtROS generation in Hepa 1–6 cells by a microplate reader. * represents a $p < 0.05$ compared to the untreated control. (F) Quantification of caspase-3/7 activation in Hepa 1–6 cells using a microplate reader.

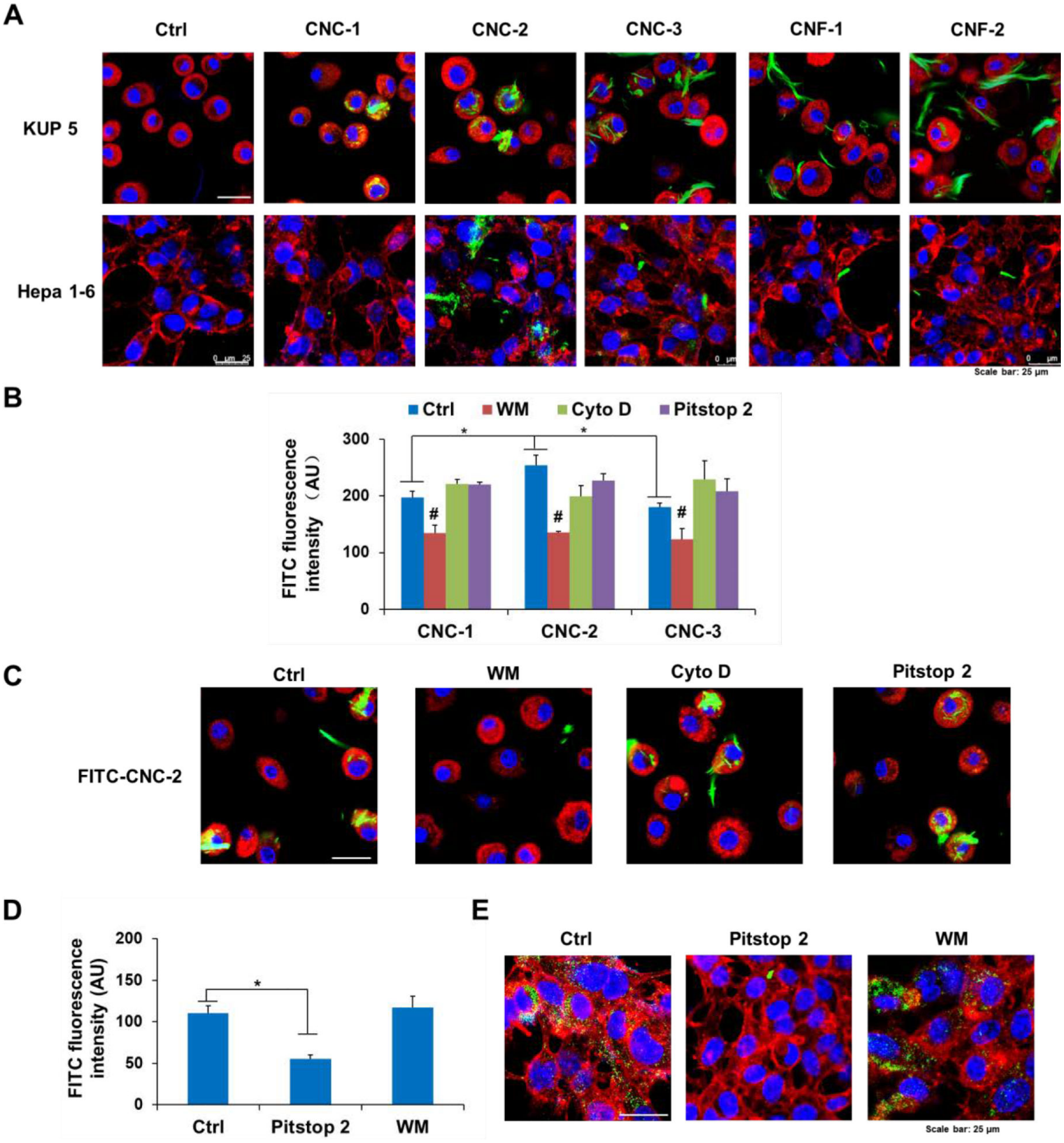
A
Ctrl
CNC-1
CNC-2
CNC-3
CNF-1
CNF-2
KUP 5
Hepa 1-6
Scale bar: 25 μm
B
Ctrl
WM
Cyto D
Pitstop 2
FITC fluorescence intensity （AU）
300
200
100
0
*
*
#
#
#
CNC-1
CNC-2
CNC-3
C
Ctrl
WM
Cyto D
Pitstop 2
FITC-CNC-2
D
FITC fluorescence intensity (AU)
200
150
100
50
0
*
Ctrl
Pitstop 2
WM
E
Ctrl
Pitstop 2
WM
Scale bar: 25 μm

Figure 4. Determination of the different cellular uptake of nanocellulose materials in KUP5 and Hepa 1–6 cells.

(A) Confocal imaging of the FITC-labeled nanocellulose materials in KUP5 (the upper line) and Hepa 1–6 cells (the lower line). These cells were incubated with 50 μg/mL of the FITC-labeled nanocellulose (green) for 16 h, followed by staining with Hoechst 33342 dyes (blue) and Alexa Fluor 594-labeled WGA antibody (red), respectively. The scale bar in the image represents 25 μm. (B) Quantification for the FITC labeled CNC-1, CNC-2, and CNC-3 incorporation in KUP5 cells and effects of inhibitors (including a phagocytosis inhibitor WM, a macropinocytosis inhibitor Cyto D, and a clathrin-dependent endocytosis inhibitor Pitstop 2) on the cellular uptake by a microplate reader. * represents a $p < 0.05$ for the comparison of CNC-2 with CNC-1 and CNC-3 treatment; # represents a p-value < 0.05

compared to the untreated control without any inhibitors. (C) Confocal images to determine the cellular localization of FITC-CNC-2 in KUP5 cells under various inhibitor treatments. (D) Quantification for the FITC labeled CNC-2 incorporation in Hepa 1–6 cells pretreated with the major cellular uptake inhibitors including Pitstop 2 and WM. * represents a p-value < 0.05 compared to the untreated control without any inhibitors. (E) Confocal images to determine the cellular localization of FITC-CNC-2 in Hepa 1–6 cells under treatments with the various inhibitors.

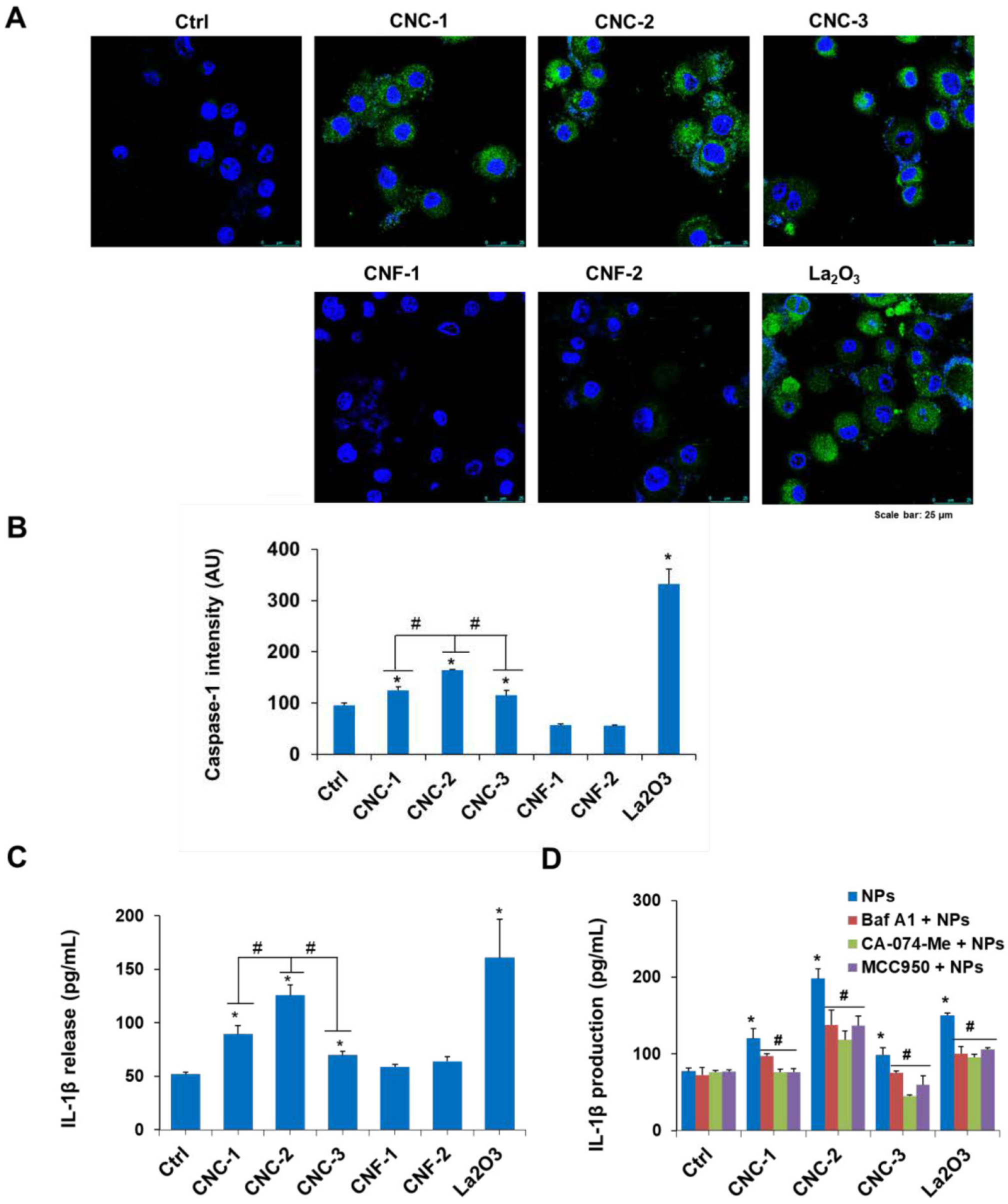

Figure 5. Determination of the lysosome damage-mediated inflammasome activation through cathepsin B release in KUP5 cells.

(A) Confocal images to compare the differences in caspase-1 activation by nanocellulose samples with various lengths in KUP5 cells. Cells were exposed to 50 µg/mL of nanocellulose samples for 16 h before staining with the FAM-FLICA caspase-1 substrate (green) for 1 h. Exposure to La$_2$O$_3$ nanoparticles, which disrupt lysosomal integrity, was used as a positive control. The scale bar in the image represents 25 µm. (B) Quantification of caspase-1 activation in cells in a microplate reader. * represents a $p < 0.05$ compared to the untreated control; # represents a p-value < 0.05 for the comparison of CNC-2 with CNC-1 and CNC-3 treatment. (C) Determination of IL-1β release in KUP5 cells after nanocellulose exposure. LPS-primed (1 µg/mL, 4 h) KUP5 cells were exposed to nanocellulose for 24 h. Supernatants were collected to measure IL-1β production by ELISA. (D) Determination of IL-1β production by CNCs (including CNC-1, CNC-2, and CNC-3) in KUP5 cells pretreated with the vacuolar H^+-ATPase (V-ATPase) inhibitor Baf A1,[41] the cathepsin B inhibitor CA-074-Me,[42] and NLRP3 inflammasome inhibitor MCC950.[43] The La_2O_3 treatment served as a positive control. * represents a $p < 0.05$ compared to the untreated control; #, $p < 0.05$ represents a significant difference compared to treatment with the nanocellulose alone.

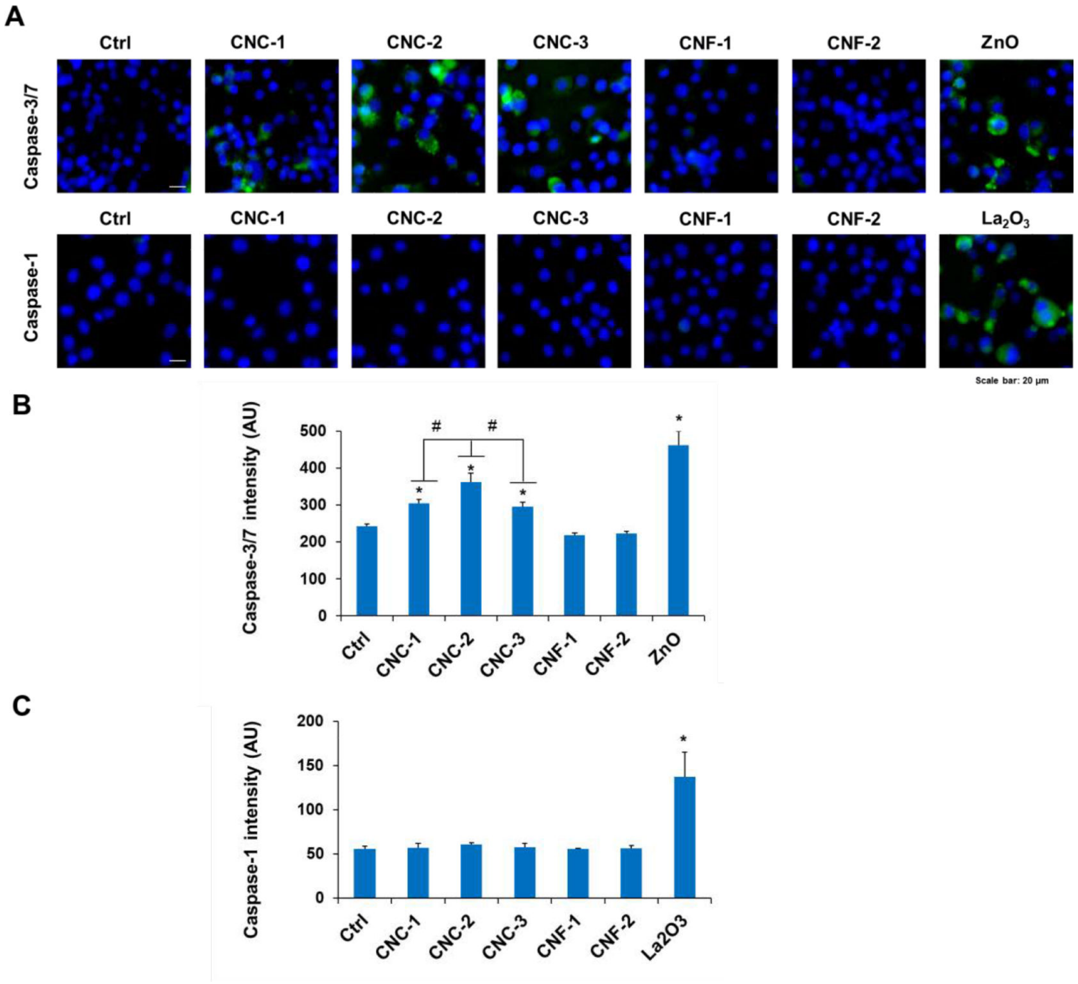

Figure 6. Comparison of the activities of caspase-3/7 and caspase-1 in KUP5 cells after various nanocellulose exposure for 5 h.

(A) Fluorescent images to determine the caspase-3/7 (the upper line) and caspase-1 (the lower line) activation in KUP5 cells exposed to various length nanocellulose materials for 5 h, respectively. The ZnO treatment was used as a positive control for caspase-3/7 activation. The La_2O_3 treatment was used as a positive control for caspase-1 activation after 5 h exposure. (B) Quantification of caspase-3/7 activation after 5 h exposure using a microplate reader. * represents a $p < 0.05$ compared to the untreated control; # represents a p-value < 0.05 for the comparison of CNC-2 with CNC-1 and CNC-3 treatment. (C) Quantification of caspase-1 activation after 5 h exposure using a microplate reader.

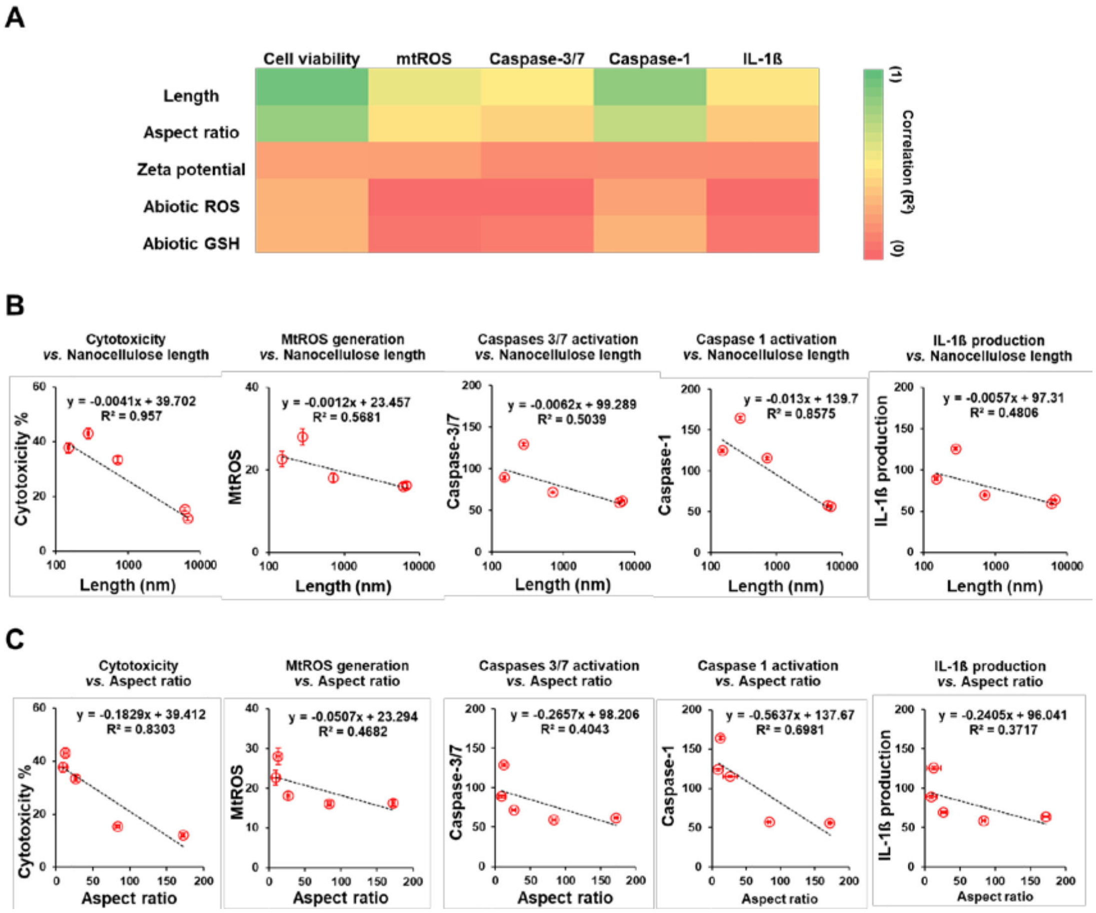

Figure 7. Determination correlations of nanocellulose physiochemical properties with the cellular responses in KUP5 cells.

(A) Heat map to demonstrate the correlations of nanocellulose length, zeta potential, abiotic ROS, and GSH level, with cellular responses in cells, including cytotoxicity, mtROS generation, caspase-3/7 activation, caspase-1 activation, and IL-1β release. The color is shown base on their correlation (R^2) and the color scale in the sidebar on the left. (B) The correlation plots of nanocellulose length against the corresponding cellular responses. (C) The correlation plots of nanocellulose aspect ratio against the corresponding cellular responses.

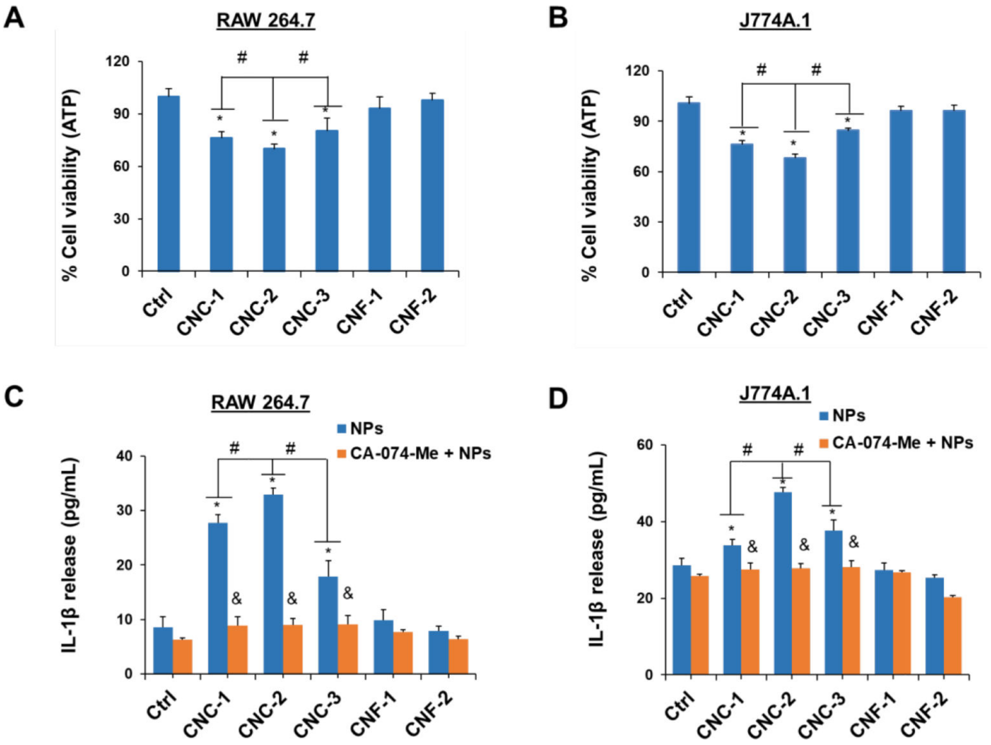

Figure 8. Determination of length-dependent toxicity (A-B) and inflammatory responses (C-D) induced by 50 μg/mL of nanocellulose in other macrophages including RAW 264.7 (A, C) and J774A.1 (B, D) cell lines.

The cathepsin B inhibitor, CA-074-Me, was used to demonstrate the cathepsin B-mediated role in the inflammatory responses in RAW 264.7 and J774A.1 cells. * represents a $p < 0.05$ compared to the untreated control; # represents a p-value < 0.05 for the comparison of CNC-2 with CNC-1 and CNC-3 treatment. &, $p < 0.05$ shows a significant difference compared to treatment with the nanocellulose alone.

Table 1.

Characterization of primary length and diameter of nanocellulose samples provided by Consortium

Sample	Length (nm)	Diameter (nm)	Aspect ratio	Source
CNC-1	149.0 ± 50.0	16.0 ± 5.0	9.3 ± 1.9	Consortium
CNC-2	279.1 ± 116.3	22.4 ± 7.2	12.7 ± 2.2	Consortium
CNC-3	715.0 ± 315.0	27.0 ± 8.0	26.5 ± 5.9	Consortium
CNF-1	6091 ± 2732	72.6 ± 63.6	83.4 ± 51.5	Consortium
CNF-2	6710 ± 5610	38.7 ± 33.4	172.1 ± 105.8	Consortium

Table 2.

Hydrodynamic size and zeta potential of nanocellulose samples in DI H_2O and DMEM cell culture medium, respectively.

Sample	Hydrodynamic size (nm)		Zeta potential (mV)	
	DI H_2O	DMEM	DI H_2O	DMEM
CNC-1	110.1 ± 11.2	121.9 ± 19.9	−38.73 ± 1.2	−14.3 ± 1.6
CNC-2	174.5 ± 30.1	249.5 ± 44.8	−34.3 ± 1.1	−12.8 ± 1.5
CNC-3	573.5 ± 20.7	780.2 ± 57.7	−30.07 ± 2.3	−11.7 ± 1.2
CNF-1	3188.6 ± 192.6	5354.2 ± 1897.5	−35.31 ± 0.2	−12.3 ± 2.0
CNF-2	3387.3 ± 371.7.0	5590.5 ± 3676.4	−27.93 ± 1.5	−11.0 ± 2.6